



Supporting Online Material for

Folding DNA into Twisted and Curved Nanoscale Shapes

Hendrik Dietz, Shawn M. Douglas, William M. Shih*

*To whom correspondence should be addressed. E-mail: william_shih@dfci.harvard.edu

Published 7 August 2009, *Science* **325**, 725 (2009)

DOI: 10.1126/science.1174251

This PDF file includes:

Materials and Methods

SOM Text

Figs. S1 to S26

References

Guide to the Supporting Online Material

Note S1:	Methods.
Note S2:	DNA toy model for designing desired bend angles.
Note S3:	What is the minimum step size for tuning bend angles?
Note S4:	Origin of stripy particle appearance in transmission electron contrast.
Note S5:	Caption to Supporting Figure 1
Supporting Figure 1:	DNA toy model for designing desired bend angles.
Supporting Figure 2:	Explanation of stripy particle appearance in transmission electron contrast.
<code><begin> separately in "1174251_SOM_figs_S3_to_S6.pdf"</code>	
Supporting Figure 3:	Zoom-out images in triplicate for the straight and the two twisting 10 by 6 helix bundles monomers and polymers discussed in main text figure 2.
Supporting Figure 4:	Zoom-out images in triplicate for each of the differently bent 3 by 6 helix bundles discussed in main text figure 3.
Supporting Figure 5:	Zoom-out images in triplicate for 6- and 12- toothed gear monomers and cyclized multimers discussed in main text figure 4.
Supporting Figure 6:	Zoom-out images in triplicate for concave and convex triangles, beachball, and spiral discussed in main text figure 4.
<code><end> separately in "1174251_SOM_figs_S3_to_S6.pdf"</code>	
Supporting Figure 7:	Detailed design schematics for the straight 10 by 6 helix bundle.
Supporting Figure 8:	Detailed design schematics for the left-twisting 10 by 6 helix bundle.
Supporting Figure 9:	Detailed design schematics for the right-twisting 10 by 6 helix bundle.
Supporting Figure 10:	Detailed design schematics for the straight 3 by 6 helix bundle.
Supporting Figure 11:	Detailed design schematics for the 3 by 6 helix bundle exhibiting a 35° bend.
Supporting Figure 12:	Detailed design schematics for the 3 by 6 helix bundle exhibiting a 30° bend.
Supporting Figure 13:	Detailed design schematics for the 3 by 6 helix bundle exhibiting a 65° bend.
Supporting Figure 14:	Detailed design schematics for the 3 by 6 helix bundle exhibiting a 60° bend.
Supporting Figure 15:	Detailed design schematics for the 3 by 6 helix bundle exhibiting a 90° bend.
Supporting Figure 16:	Detailed design schematics for the 3 by 6 helix bundle exhibiting a 120° bend.
Supporting Figure 17:	Detailed design schematics for the 3 by 6 helix bundle exhibiting a 150° bend.
Supporting Figure 18:	Detailed design schematics for the 3 by 6 helix bundle exhibiting a 180° bend.
Supporting Figure 19:	Detailed design schematics for the 6-toothed 50 nm wide gear.
Supporting Figure 20:	Detailed design schematics for the 12-toothed 100 nm wide gear.
Supporting Figure 21:	Detailed design schematics for the wireframe beach ball.
Supporting Figure 22:	Detailed design schematics for the concave triangle.
Supporting Figure 23:	Detailed design schematics for the convex triangle.
Supporting Figure 24:	Detailed design schematics for the spiral.
Supporting Figure 25:	Patterns of number-of-basepair / helix installed in the 10 by 6 helix bundles from figure 3
Sequences:	Oligonucleotide sequences for each object.

(Note S1) Methods

Folding. Assembly of DNA-origami bundles is accomplished in a one-pot reaction by mixing 20 nM scaffold strands derived from M13 bacteriophage with 120 nM of every oligonucleotide staple strands (reverse-phase cartridge purified, Bioneer Inc.) in a buffer including 5 mM TRIS, 1 mM EDTA, 18 mM MgCl₂, 5 mM NaCl (pH 8) and subjecting the mixture to a thermal-annealing ramp that cooled from 80° C to 60°C over the course of 80 minutes and then cooled from 60°C to 24°C over 173 hours.

Gel purification. Folding products were electrophoresed on 2% agarose gel containing 0.5x TBE, 11 mM MgCl₂, 0.5 µg/ml ethidium bromide at 75 V for four hours in a gel box incubated in an ice-water bath. Monomer bands were excised and DNA recovered by pestle-crushing excised bands followed by centrifugation for 10 min at 16000 rcf at 4°C using Freeze 'N Squeeze DNA Gel Extraction spin columns (Bio-Rad). Recovered material in the flow-through was stored at 4°C for further use.

Transmission electron microscopy. For imaging, particles were adsorbed onto glow-discharged collodion- and carbon-coated TEM grids and then stained using a 2% aqueous uranyl formate solution containing 25 mM NaOH. Imaging was performed using an FEI Tecnai T12 BioTWIN operated at 120 kV.

Recombinant M13 filamentous bacteriophage construction. Recombinant phages were prepared by replacement of the BamHI-XbaI segment of M13mp18 by PCR-amplified fragments of bacteriophage λ DNA. Double-stranded (replicative form) bacteriophage M13 DNA bearing inserts were prepared as described [S1]. Inserts were verified by restriction double digest using BamHI and XbaI, followed by DNA sequencing. Single-stranded bacteriophage M13 DNA was prepared as described in [S2].

(Note S2) DNA toy model for designing desired bend angles.

In our toy model, we consider the total energy stored in a DNA-origami bundle as a sum of bend, stretch/compression, and twist-stretch coupling contributions stored in each base pair in the bundle. We consider DNA-origami bundle segments with the following properties: (a) the segment begins and ends on crossover planes, (b) the segment has a fixed cross-section geometry along the helix-parallel axis, (c) base-pair additions and deletions between crossover planes are dispersed as uniformly as possible along the segment's helix-parallel axis to yield an approximately constant gradient of local twist density, and (d) deletions and insertions are balanced so as to maintain an overall average twist density of 10.5 base-pairs-per-turn (bp/turn).

$$E_{total} = \sum_i \frac{1}{2} S \cdot n_i \frac{(d_i - d_{eq})^2}{d_{eq}} + \frac{1}{2} B \cdot n_i \frac{d_{eq}}{(r_0 + \delta_i)^2} + \frac{1}{2} D \cdot \phi_i \left(\frac{d_i}{d_{eq}} - 1 \right) \quad (1)$$

$$d_i = \frac{n_0}{n_i} \cdot d_0 \left(\frac{\delta_i}{r_0} + 1 \right) \quad (2)$$

$$\phi_i = 2\pi \cdot \frac{N - n_i}{10.5} \quad (3)$$

In equation (1), the index i runs over all helices in the bundle (see Fig. S1 E for a scheme). S , B , and D denote the stretch, bending, and twist-stretch-coupling moduli of DNA [S3, S4]; r_0 denotes the radius of curvature of a reference helix in the bundle, the term $(r_0 + \delta_i)$ provides the radius of curvature of the i -th helix. Here, the DNA bundle's cross-section geometry enters the model as a parameter.

The numbers n_i describe the net number of base pairs that are installed on each helix in the bundle segment between the limiting crossover-array planes and describe the cross-sectional pattern of insertions and deletions that is imposed to induce bending.

The number d_{eq} denotes the unperturbed length-per-base-pair in B-form DNA, while d_i refers to the average length per base pair occurring on the i -th helix in the DNA bundle when it is bent. Every helix in the bundle is forced to subtend the same central angle between the two limiting crossover planes regardless of the number of base pairs installed on each particular helix. Hence, the numbers d_i all can be expressed relative to the length-per-base-pair d_0 occurring on a chosen reference strand by using equation (2).

Finally, ϕ_i describes cumulative twist arising in the i -th helix in the bundle when deviating from the default number of base pairs N and is obtained by using equation (3), (e.g. N equals 98 between 15 crossover planes).

Important geometric parameters for the toy model are the unperturbed length-per-base-pair d_{eq} and the effective diameter of each helix in the DNA bundle. We determined these parameters experimentally by measuring the width and length of a straight, unperturbed 3 by 6 helix bundle version with 10.5 bp/turn double-helical twist density by single-particle analysis in negative stain transmission electron microscopy (see Figs. S1A-S1C). We obtained a length/bp $d_{eq}=0.335\pm(0.007 \text{ s.d.})$ nm, in very good accordance with recent solution measurements on DNA [S5]. For the effective helix diameter, we obtained a value of $2.25\pm(0.01 \text{ s.e.m.})$ nm.

The energetic contributions in equation (1) are scaled by a set of parameters that describe the mechanical properties of a single DNA double helix. We used two different sets of parameters, one that includes twist-stretch coupling ($S=1100$ pN, $B=230$ pN \cdot nm², $D=-90$ pN \cdot nm) [S4] and another set ($S=660$ pN, $B=230$ pN \cdot nm², $D=0$ pN \cdot nm) excluding twist-stretch coupling and with S and B calculated via a Young's modulus derived from a DNA persistence length of 50 nm and our experimentally observed effective helix diameter.

We sampled the total energy as a function of curvature $1/r_0$ and length/bp d_0 on the reference strand. An example energy landscape is shown in Fig. 1G. The bend angle θ subtended by the bent bundle at any point on this energy surface can be obtained via

$\theta = n_0 \cdot d_0 / r_0$. We applied Boltzmann-weighted statistics to compute probability density distributions for observing a certain central bend angle θ . Example distributions resulting from calculations with and without twist-stretch coupling contributions are displayed in Fig. S1D, together with histograms of experimentally observed bend angles as discussed in the main text. Our toy model predicts thermally induced angular deviations of about 2.5° from the respective minimum-energy bend angle. Fig. S1F provides a more detailed comparison of our toy model with the experimentally observed bending. Interestingly, at lower bend angles, our experiments show that the corresponding DNA bundles actually bend more than the model would predict, while for high bend angles the toy model predicts more bending than actually takes place. Estimations when including twist-stretch coupling perform better particularly for high bend angles. It will be an important task for the future to refine the model, to study quantitatively the effect of defects on expected bending, and also to sample degrees of freedom describing global twist.

(Note S3) What is the minimum step size for tuning bend angles?

To address this question, Figs. S1H and S1I provide two examples for 3 by 6 helix bundles that have been designed to bend by 30° and 60° (red histograms and red cross-section schemes). The average bend angles were observed to be $30.7^\circ \pm 5.4^\circ$ (N=212) and $62.4^\circ \pm 5.9^\circ$ (N=208). We changed the net number of base pairs in three out of the six cross-section layers by adding or deleting only one base pair (gray cross-section) and again analyzed the bend angles of the altered versions (gray histograms). As a result, we observed an angular shift of about 5° to produce mean bend angles of $34^\circ \pm 5^\circ$ (N=213) and $67.5^\circ \pm 5.7^\circ$ (N=244),

which is a shift of about one standard deviation away from the previous bend angle. An even finer tuning most likely will be possible by altering the base-pair content in the individual different layers of the bundle's cross-section that one intends to bend.

(Note S4) Origin of stripy particle appearance in transmission electron contrast.

To address this question, Fig. S2 shows a cross-sectional slice of a 3 by 6 helix bundle where each helix is depicted as a simple cylinder. By integrating the image intensities from top-to-bottom, one obtains an intensity profile exhibiting three pronounced peaks (bottom right), while a projection from right-to-left yields a much smoother profile with many smaller peaks that are washed out in noisy negative stain transmission electron micrographs, thus providing an explanation for why the 3 by 6 helix bundles either exhibit three pronounced stripes or a smooth appearance along the bundle length when imaged with a transmission electron microscope. The 'stripy' view is perpendicular to the direction of the gradient of insertions and deletions installed in the 3 by 6 helix bundles and bending occurs parallel to the image plane. The stripes therefore serve as a selection criterion to identify the subset of particles that adhered to the electron microscope imaging surface in an orientation that allows for directly assessing their bending behavior.

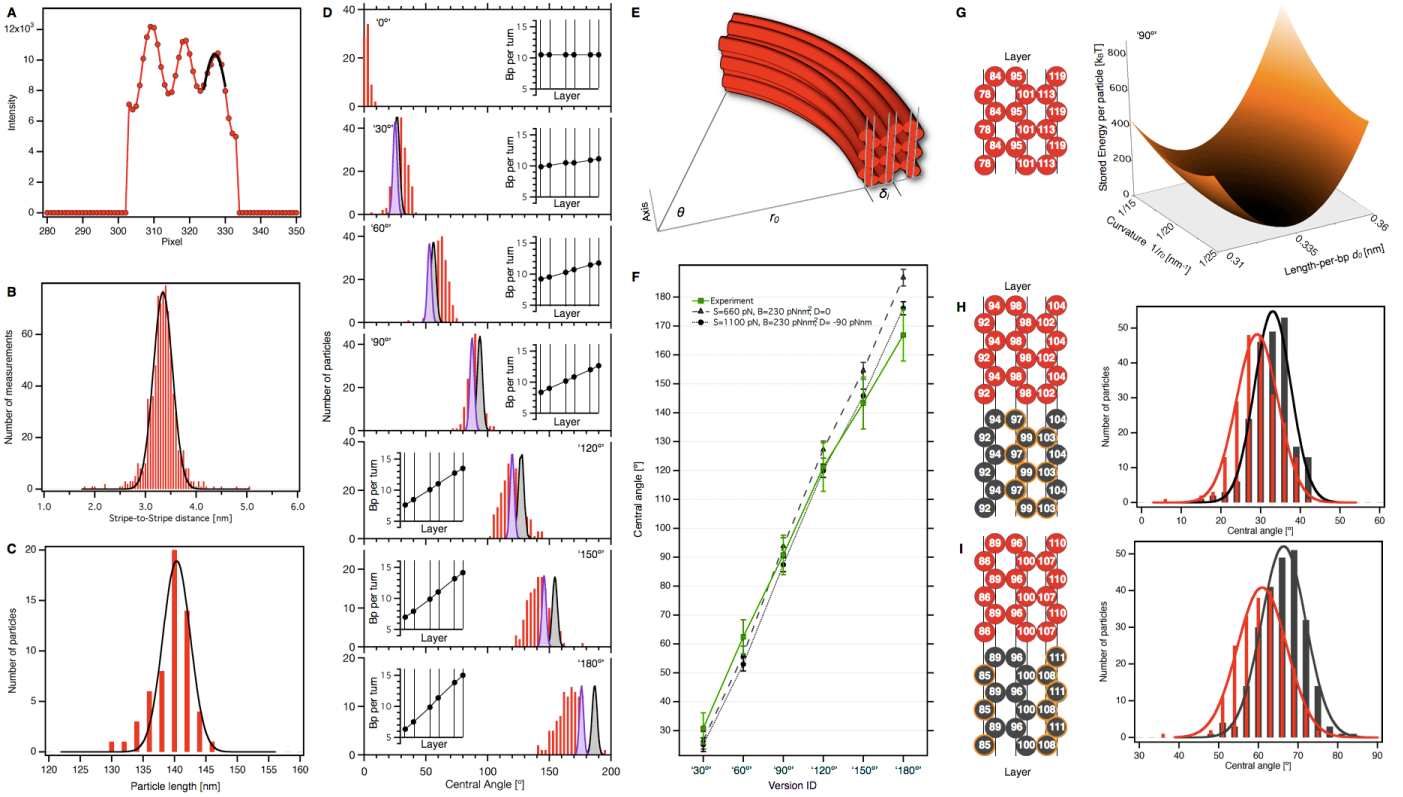
(Note S5) Caption to Supporting Figure S1

Supporting Figure 1. Quantitative prediction of bend angles. **(A)** Line-intensity profile (red) of a non-bent 3 by 6-helix bundle as obtained from negative-stain TEM (see Fig. 4), integrated over a 10-pixel-long box along particle's helix-parallel axis. A Gaussian fit to determine 'stripe' position is shown in black. **(B)** Histogram of stripe-to-stripe distances. Average distance is $3.37 \pm (0.01 \text{ s.e.m.}) \text{ nm}$ ($N=782$), corresponding to an average effective helix diameter of 2.25 nm in the 3 by 6-helix bundle. Gaussian fit shown as black line. **(C)** Histogram of the observed length of the non-bent 3 by 6-helix bundles as obtained from single particles in negative-stain TEM micrographs. Average length is $140 \pm (3 \text{ s.d.}) \text{ nm}$ ($N=58$). The 3 by 6-helix bundles are 420 bp long, hence length/bp is $0.335 \pm (0.007 \text{ s.d.}) \text{ nm}$. Gaussian fit shown as black line. **(D)** Histograms (red bars) of observed bend angles for the seven 3 by 6-helix bundle versions discussed in the main text. Imposed double-helical-twist-density plot (inset graphs) through the 3 by 6-helix-bundle cross section resulting from the implemented patterns of insertions and deletions. The predicted bend-angle distributions derived from toy models that include bending and stretch/compression contributions (black peaks) and bending, stretch/compression, and negative twist-stretch coupling (purple peaks) contributions. **(E)** Scheme of experimental geometry. **(F)** Detailed comparison of experiment with predictions of the toy models. Predicted and observed mean bend angles are plotted for each design, with standard deviations shown as bars. **(G)** An example 3 by 6 helix bundle cross section, labeled with content of base pairs located between 15 crossover planes that comprise the bent segment (i.e. what would normally be 98 base pairs). Corresponding energy landscape as a function of the parameters curvature and length/bp. This particular design realizes an experimentally observed bend angle of $91.3^\circ (\pm 5.2^\circ \text{ s.d.})$ (see Fig. 4D, main text). **(H, I)** Two pairs of 3 by 6-helix cross-sections and corresponding observed bend angle histograms showing the bend angle increase resulting from a minor design modification. Corresponding histograms for experimentally observed bend angles from single-particle shape analysis by negative-stain TEM are shown to the right. For each pair of designs, the first angle is depicted in red, and the modified angle is shown in black. Helices that are different between the paired designs are shown with an orange outline.

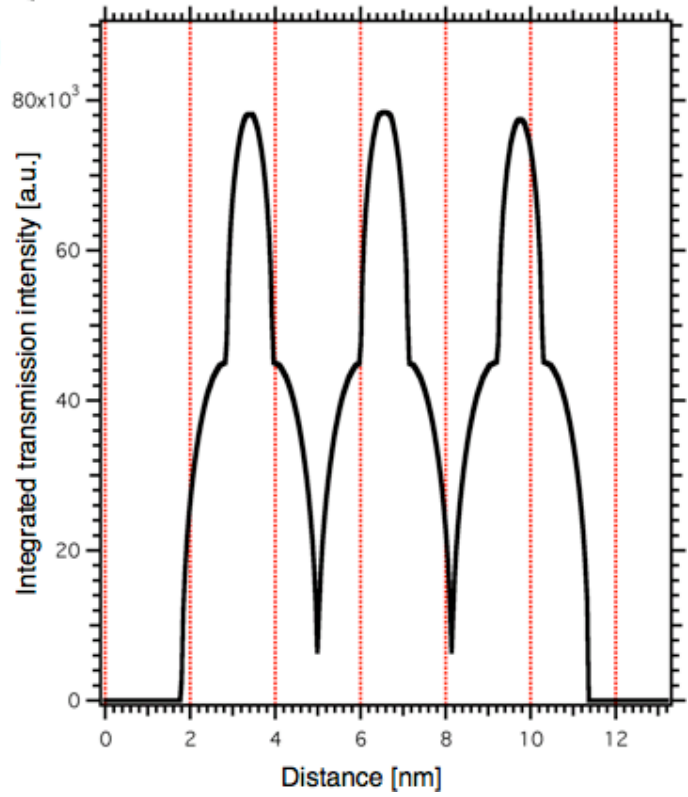
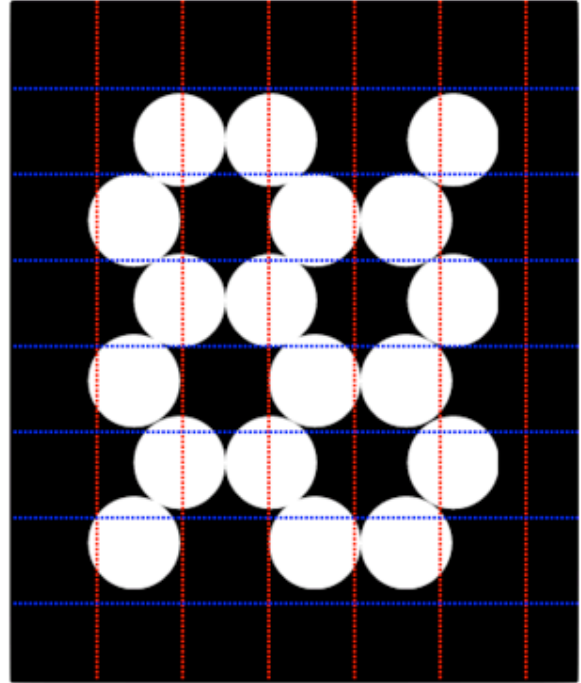
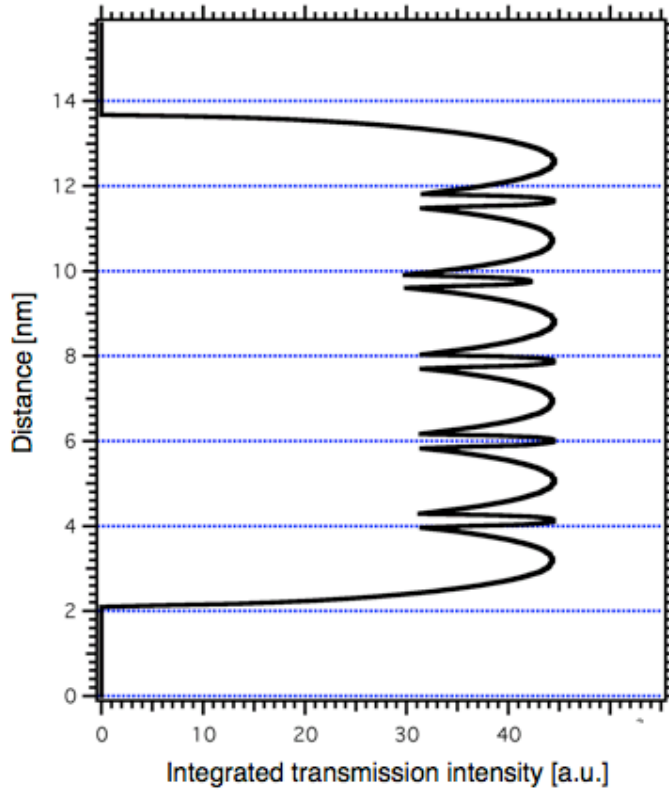
Supporting References

- S1. Sambrook, J. and D. Russell, *Molecular Cloning: A Laboratory Manual*. Third ed. 2001, Cold Spring Harbor: Cold Spring Harbor Laboratory Press.
- S2. Douglas, S.M., J.J. Chou, and W.M. Shih, DNA-nanotube-induced alignment of membrane proteins for NMR structure determination. *Proc Natl Acad Sci U S A*, 2007. **104**(16): p. 6644-8.
- S3. Bryant, Z., et al., Structural transitions and elasticity from torque measurements on DNA. *Nature*, 2003. **424**(6946): p. 338-41.
- S4. Gore, J., et al., DNA overwinds when stretched. *Nature*, 2006. **442**(7104): p. 836-9.
- S5. Mathew-Fenn, R.S., R. Das, and P.A. Harbury, Remeasuring the double helix. *Science*, 2008. **322**(5900): p. 446-9.

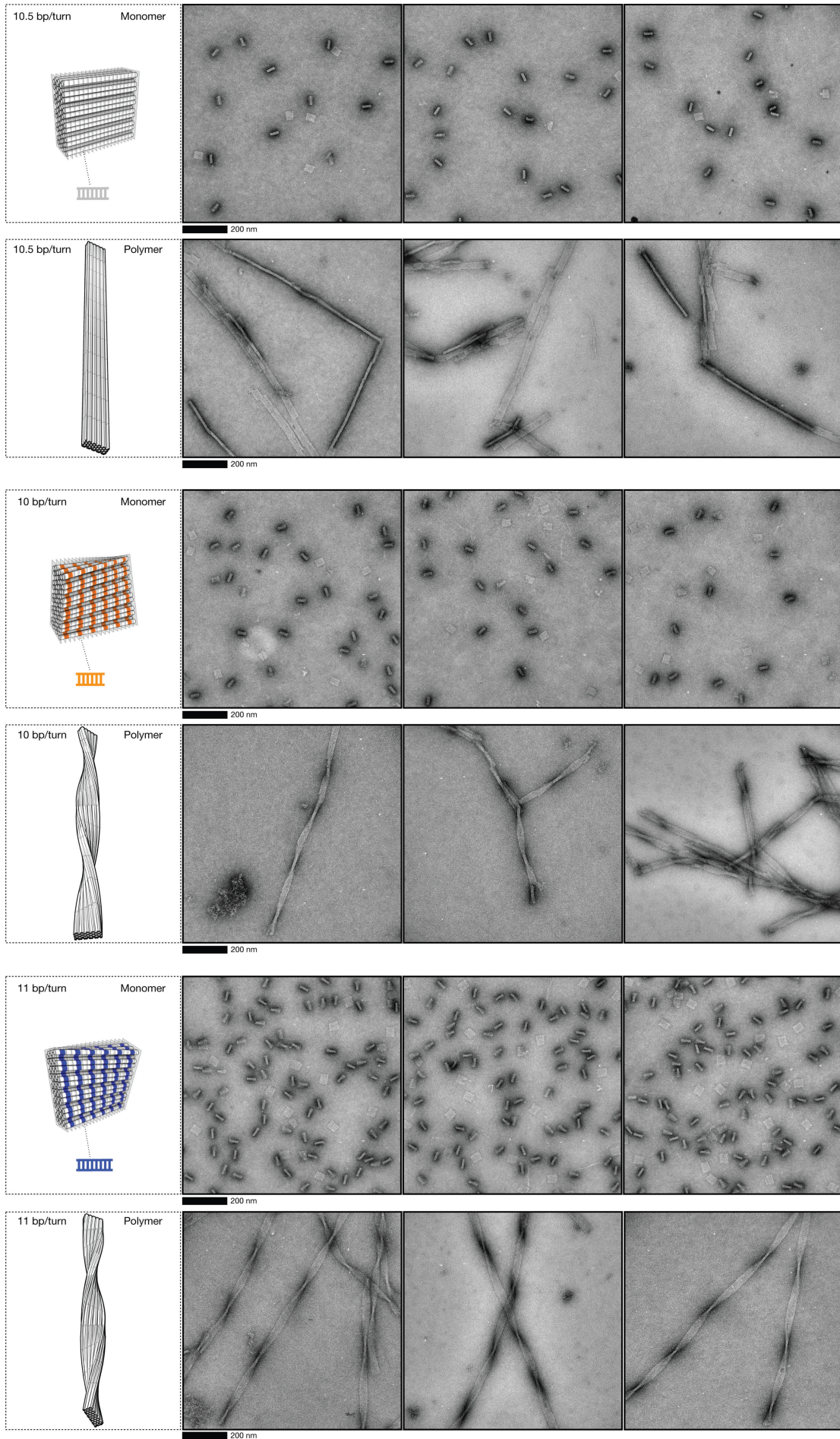
Supporting Figure 1



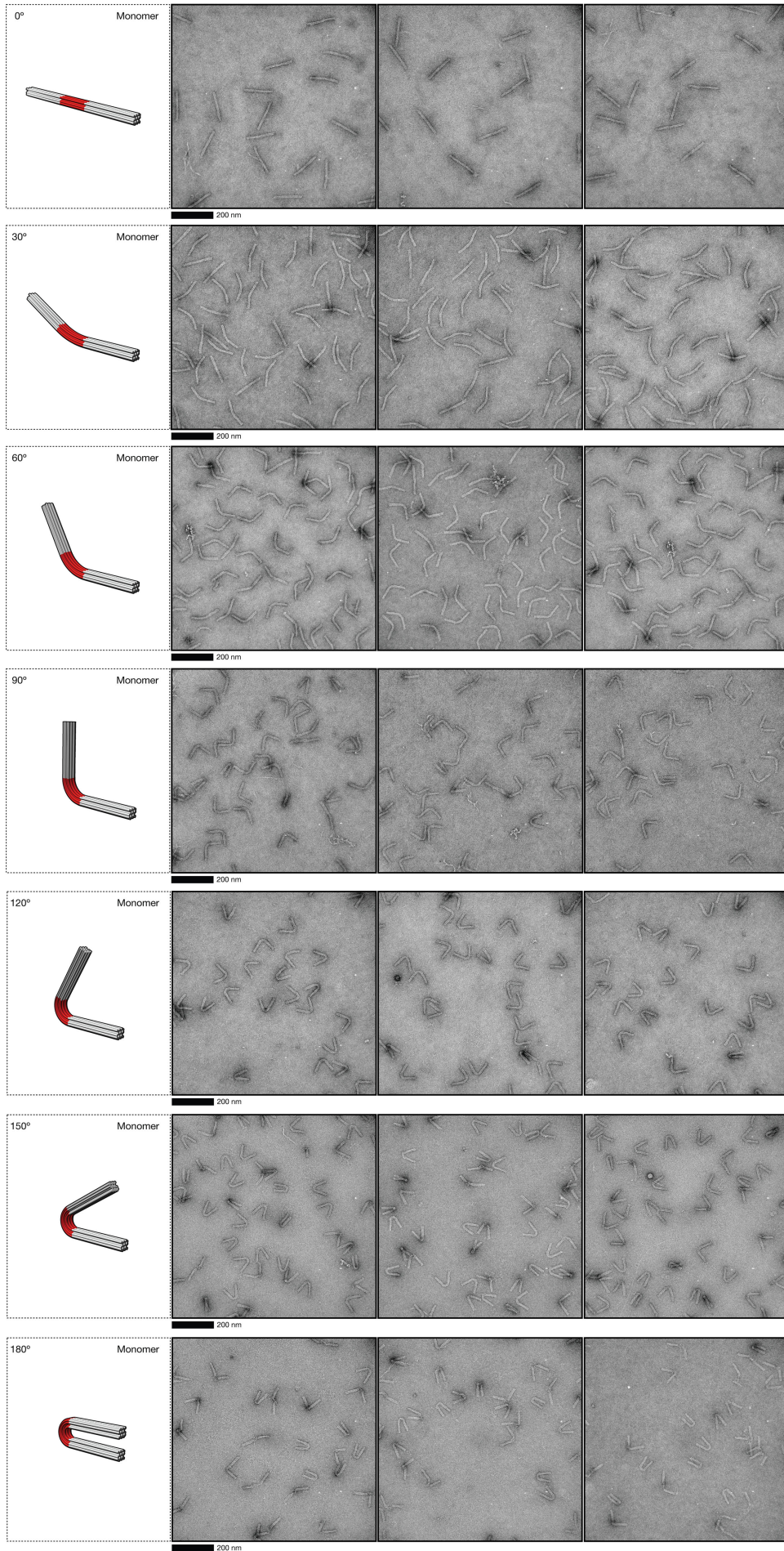
Supporting Figure 2



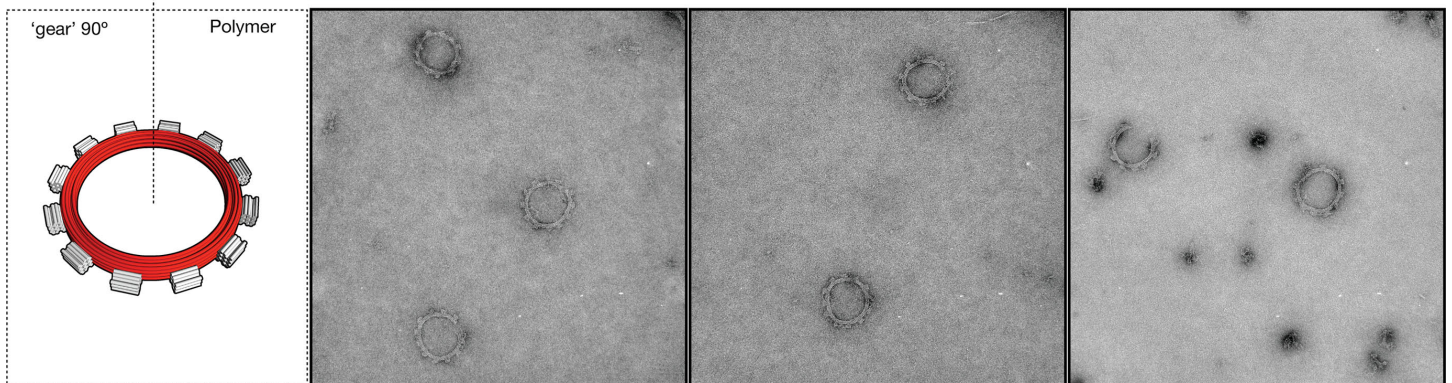
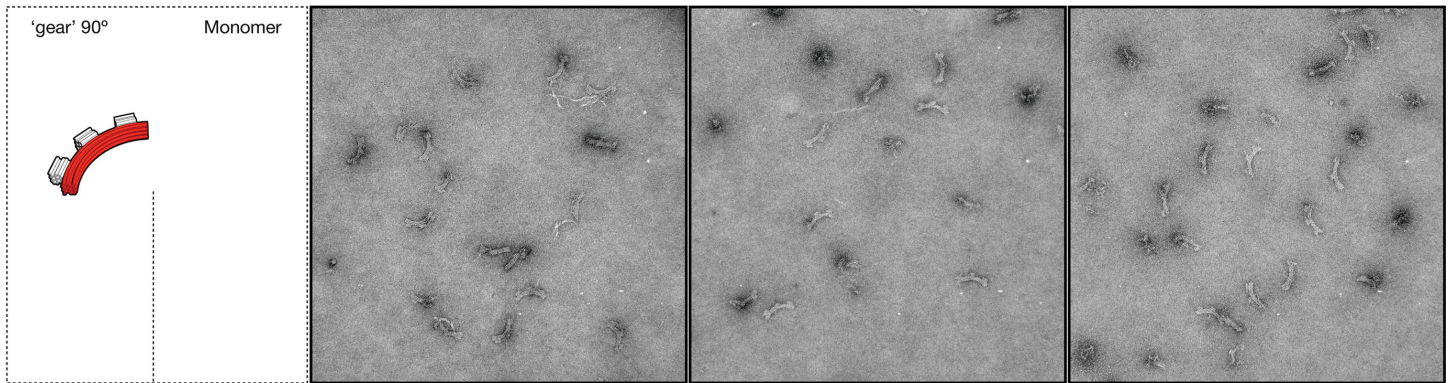
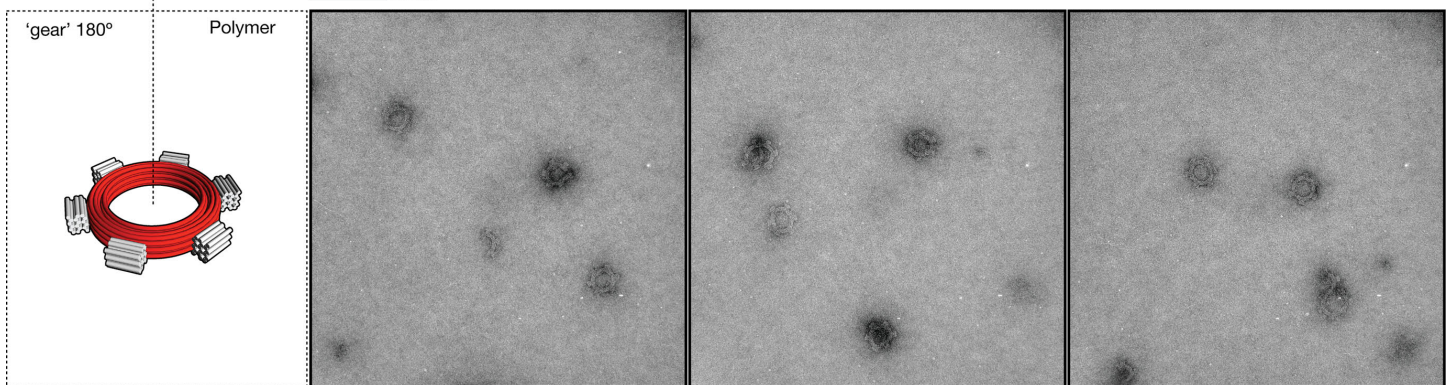
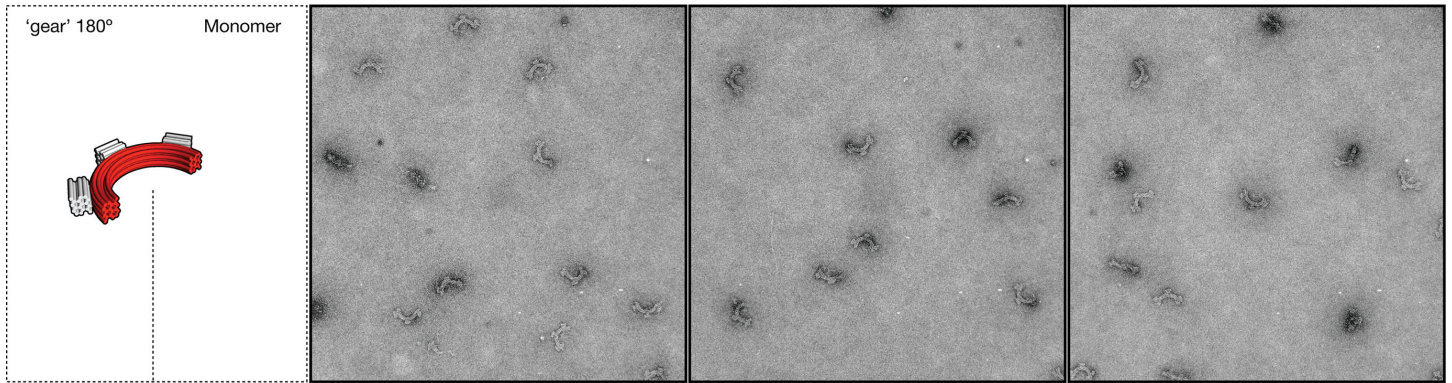
Supporting Figure 3



Supporting Figure 4

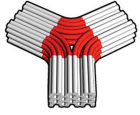


Supporting Figure 5



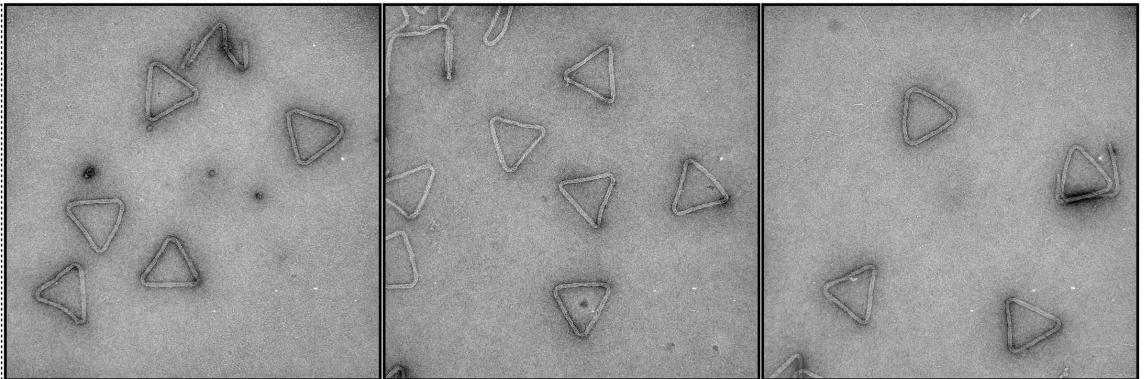
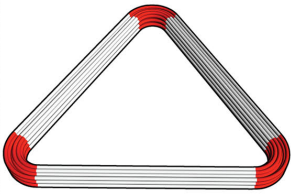
Supporting Figure 6

concave triangle Monomer



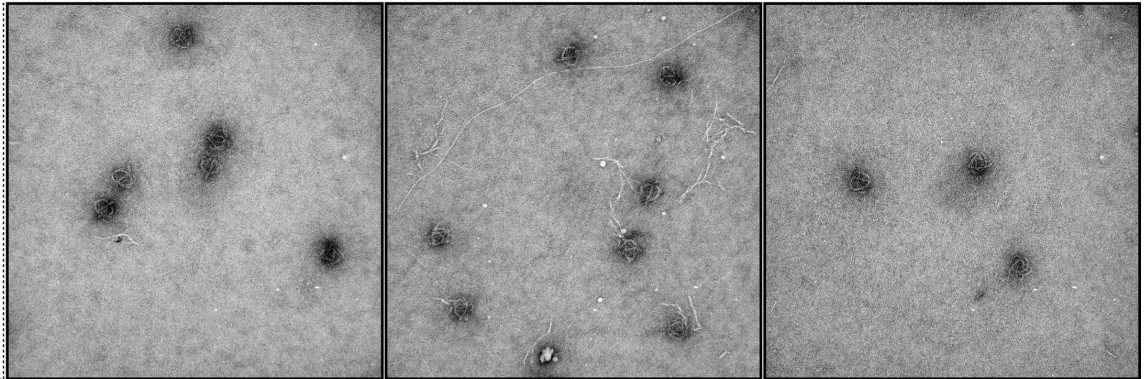
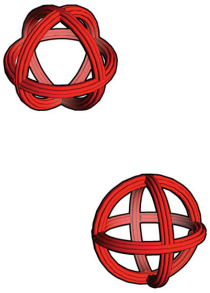
200 nm

convex triangle Polymer



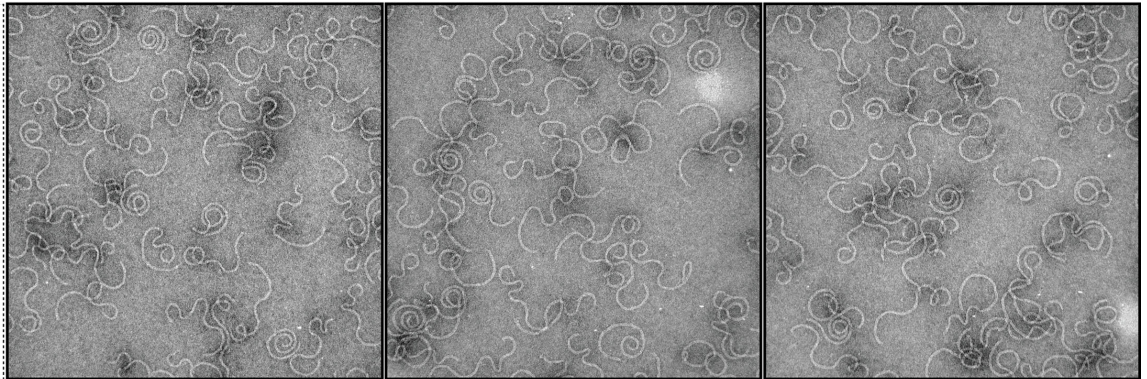
200 nm

'beach ball' Monomer



200 nm

'spiral' Monomer

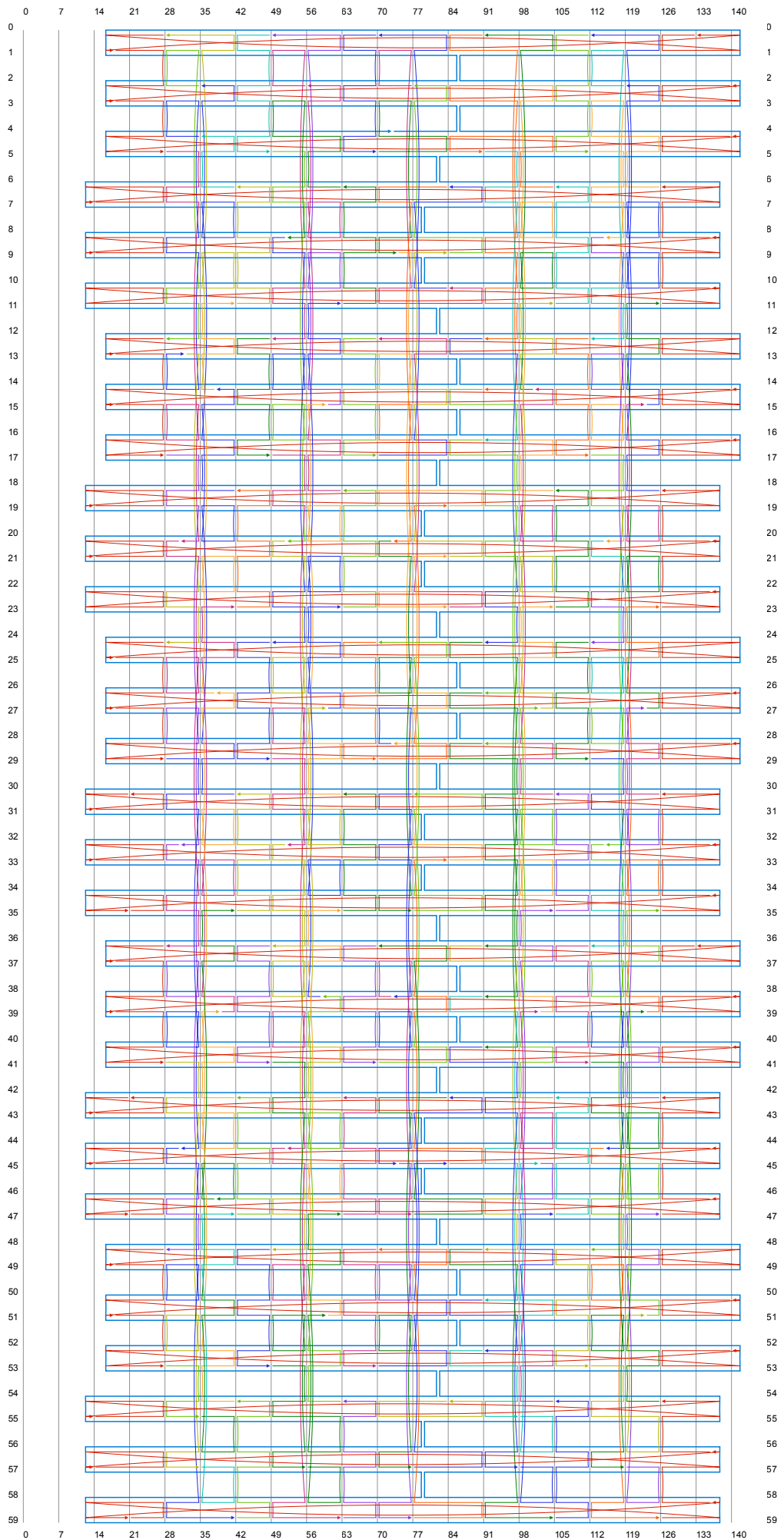
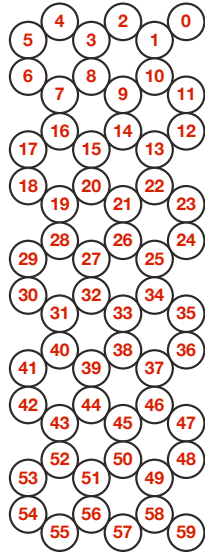


200 nm

Supporting

Figure 7

10 by 6 block
straight

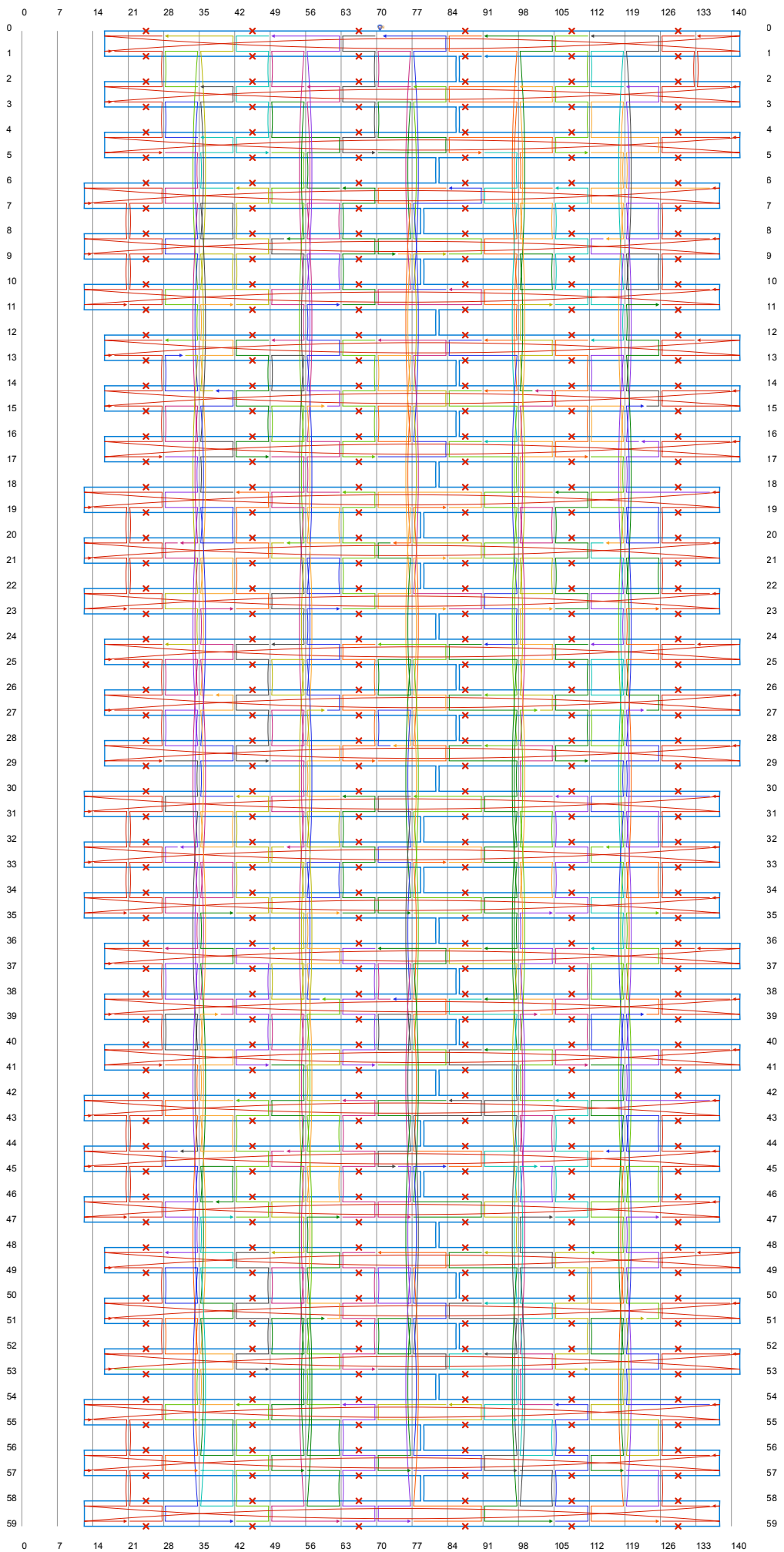
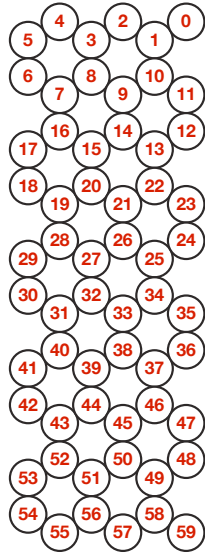


Supporting

Figure 8

10 by 6 block

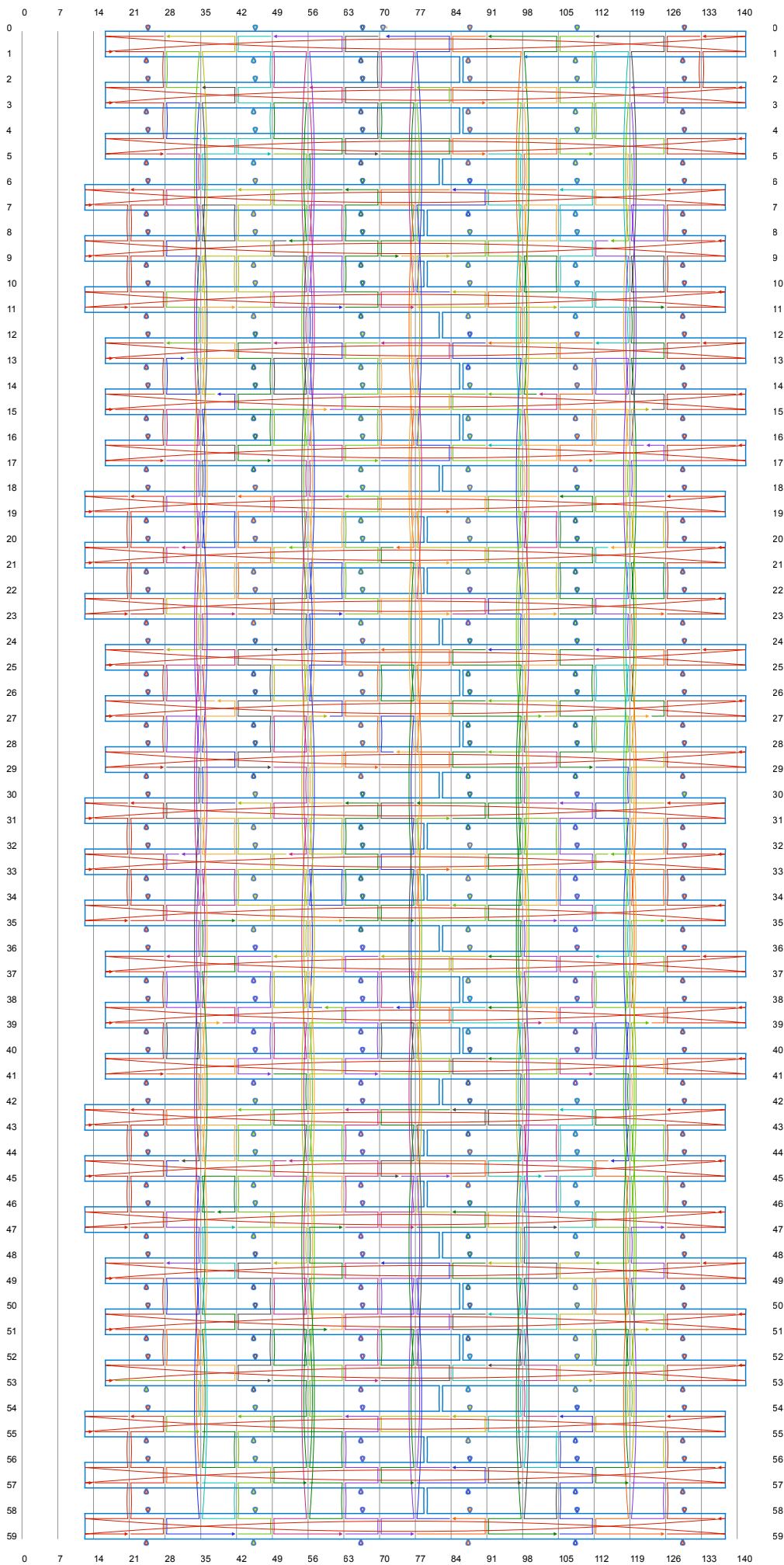
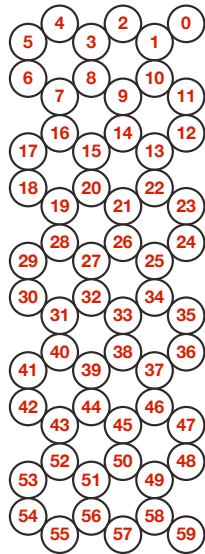
left twist



Supporting

Figure 9

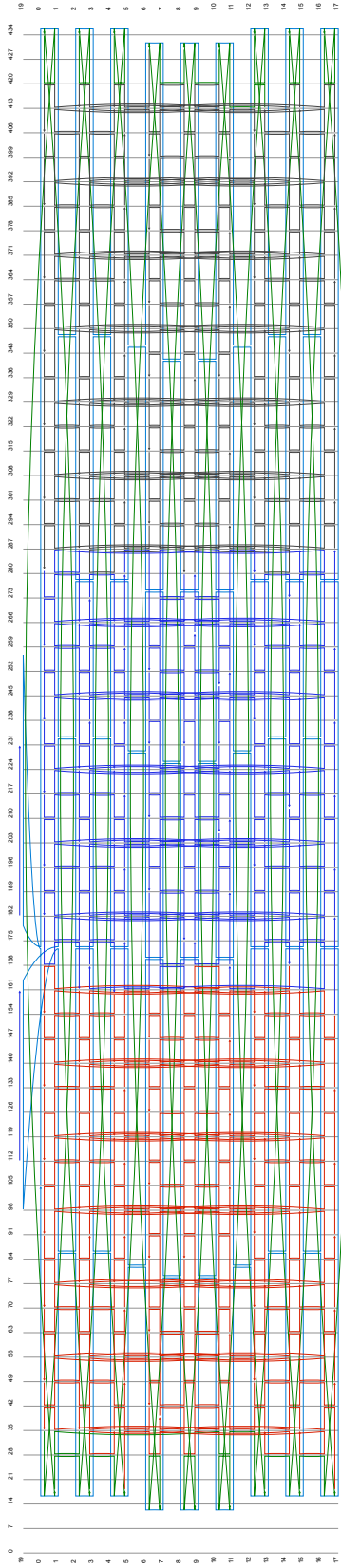
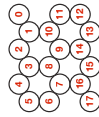
10 by 6 block
right twist



Supporting Figure 10

3 by 6 block

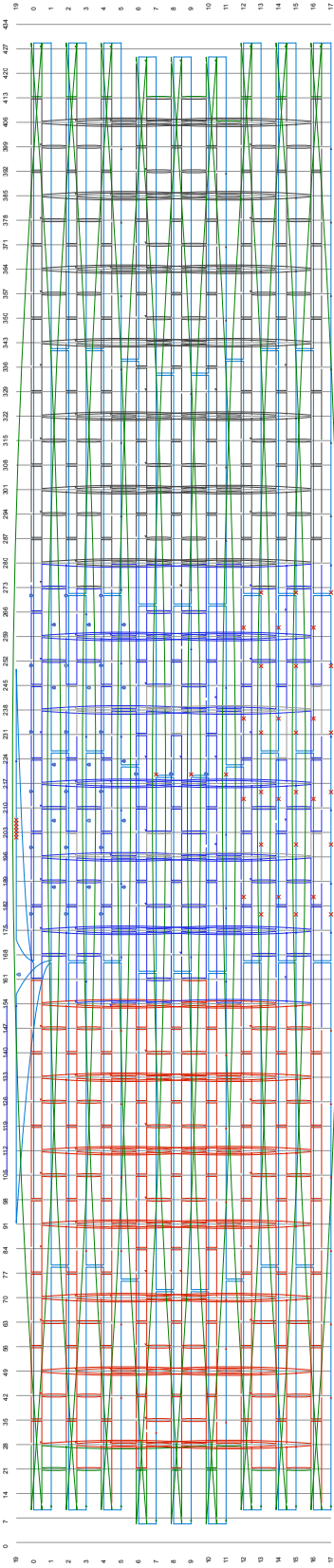
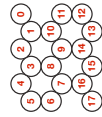
0° bend

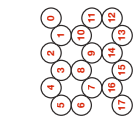


Supporting Figure 11

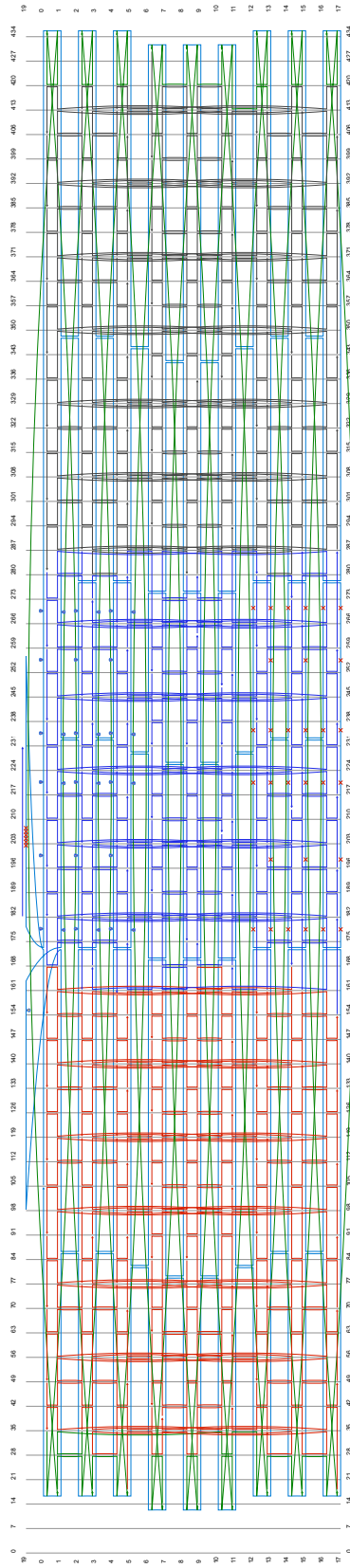
3 by 6 block

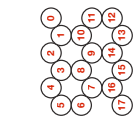
35° bend



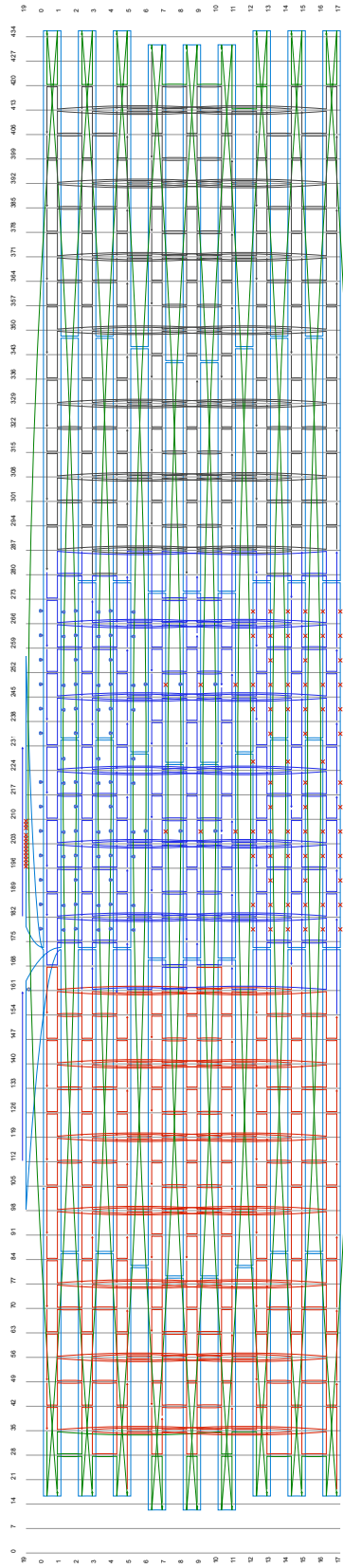


Supporting Figure 12
 3 by 6 block
 30° bend





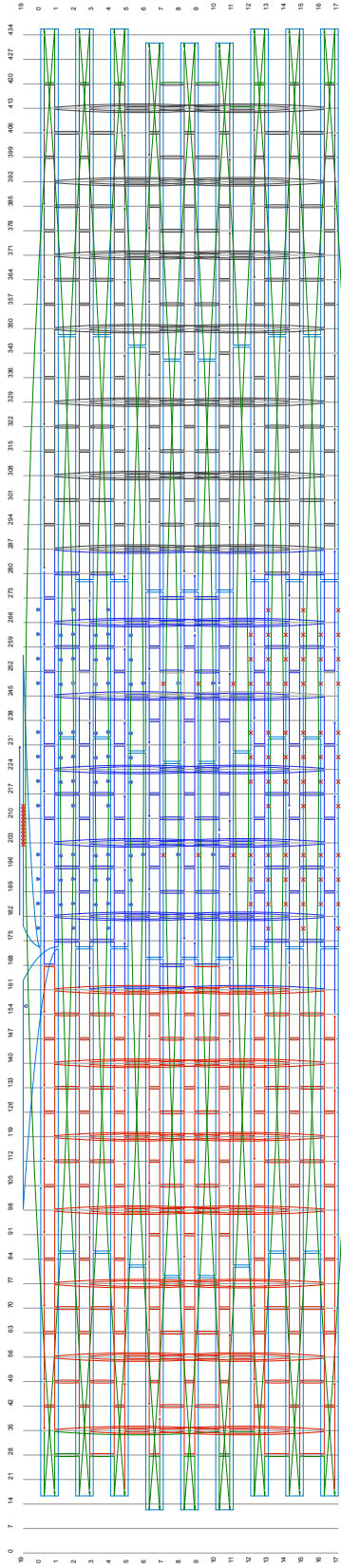
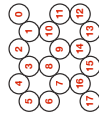
Supporting Figure 13
 3 by 6 block
 65° bend



Supporting Figure 14

3 by 6 block

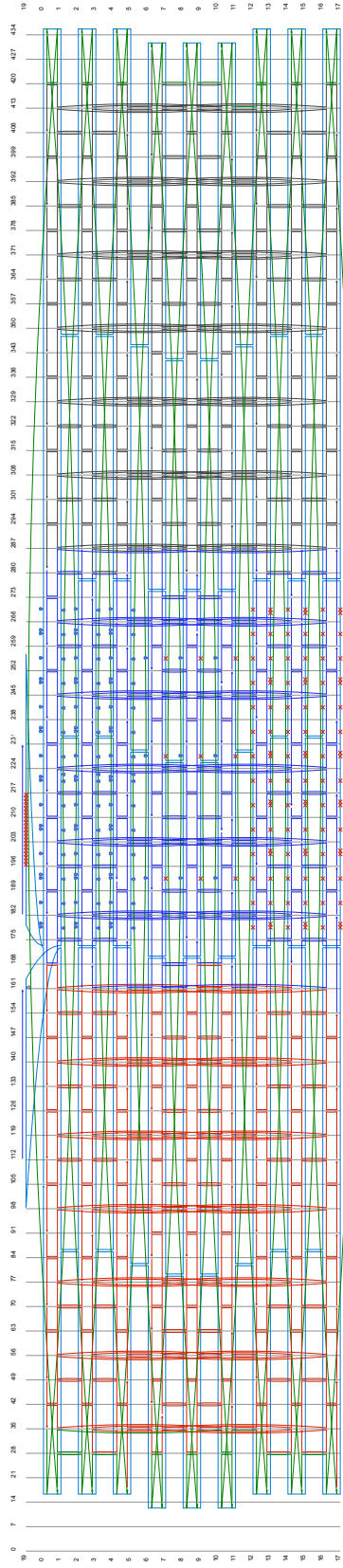
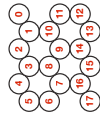
60° bend

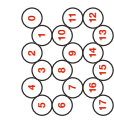


Supporting Figure 15

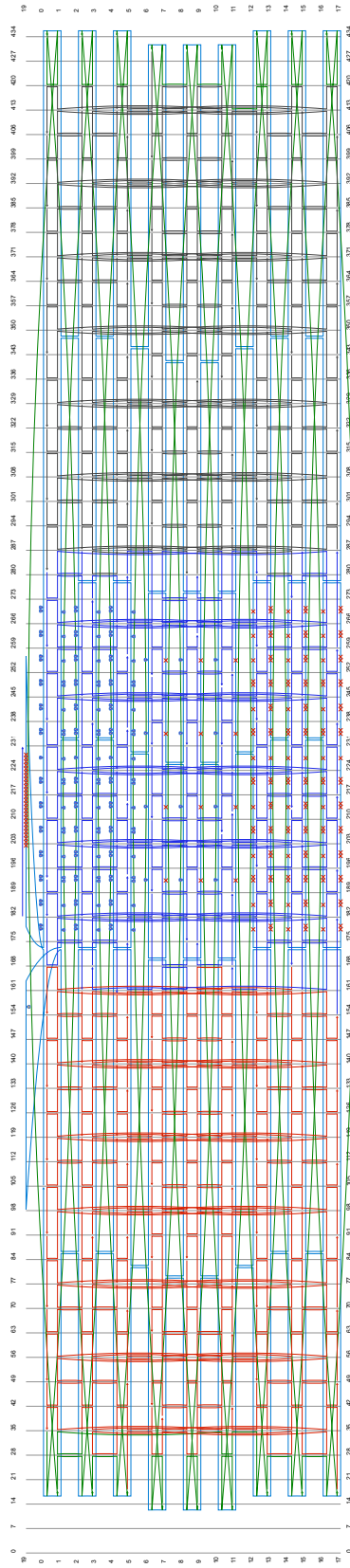
3 by 6 block

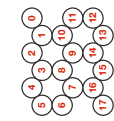
90° bend



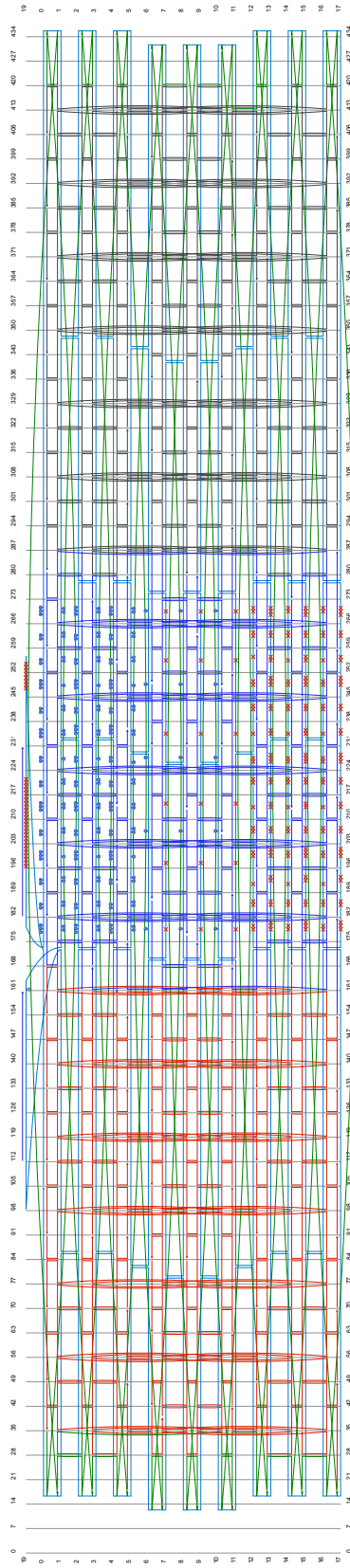


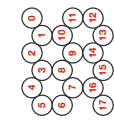
Supporting Figure 16
 3 by 6 block
 120° bend



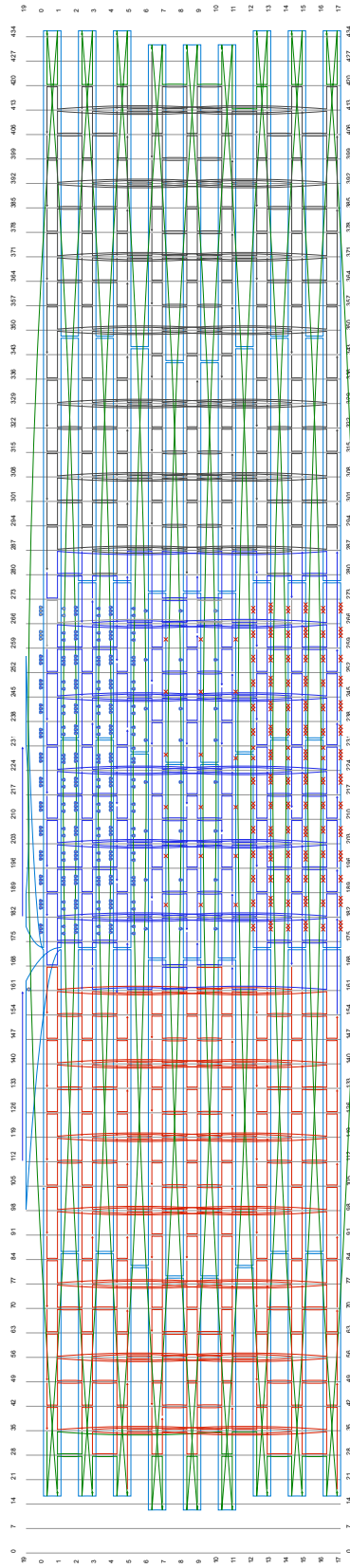


Supporting Figure 17
 3 by 6 block
 150° bend





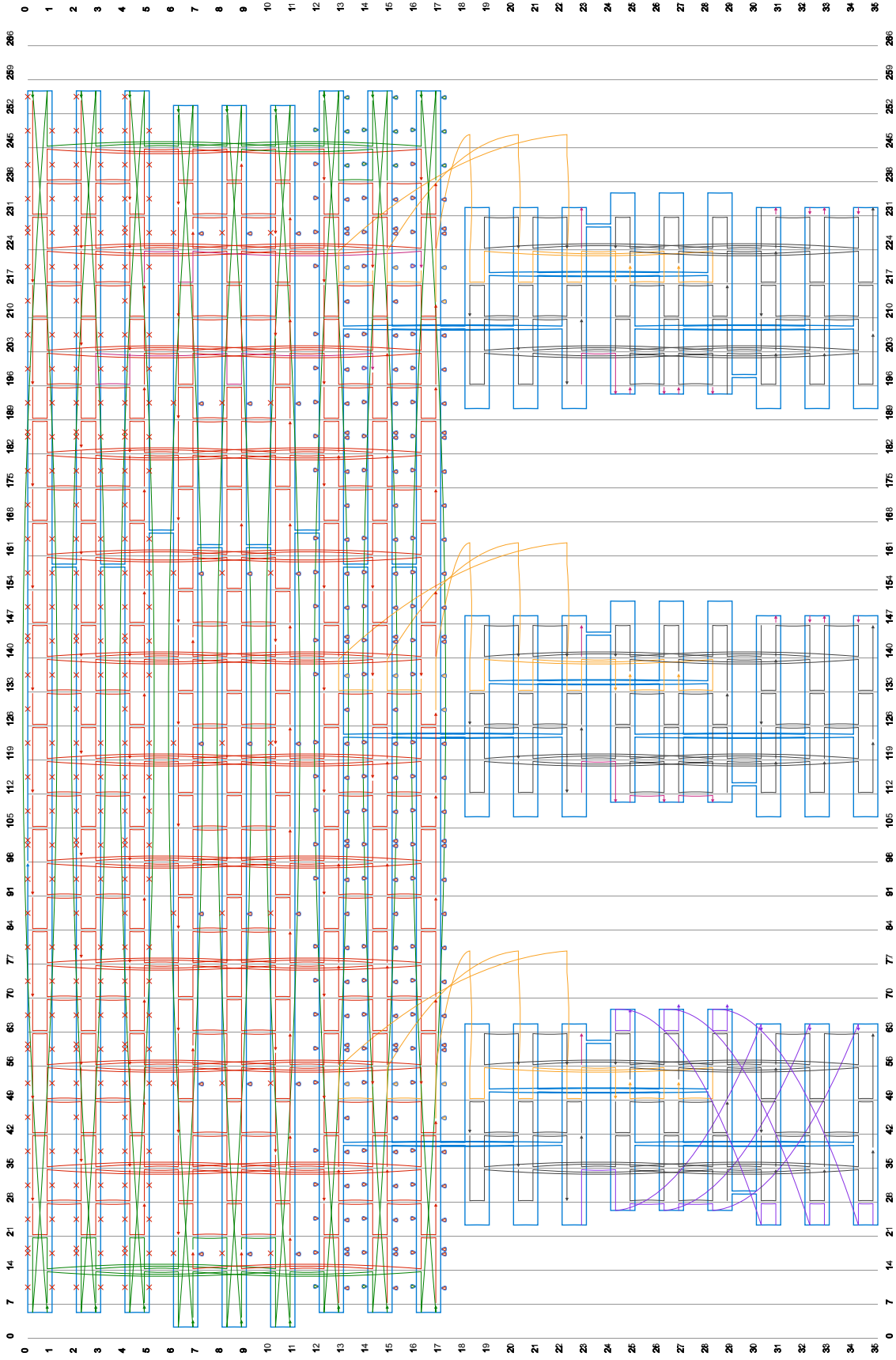
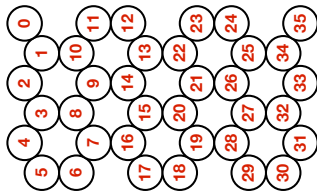
Supporting Figure 18
 3 by 6 block
 180° bend



Supporting

Figure 19

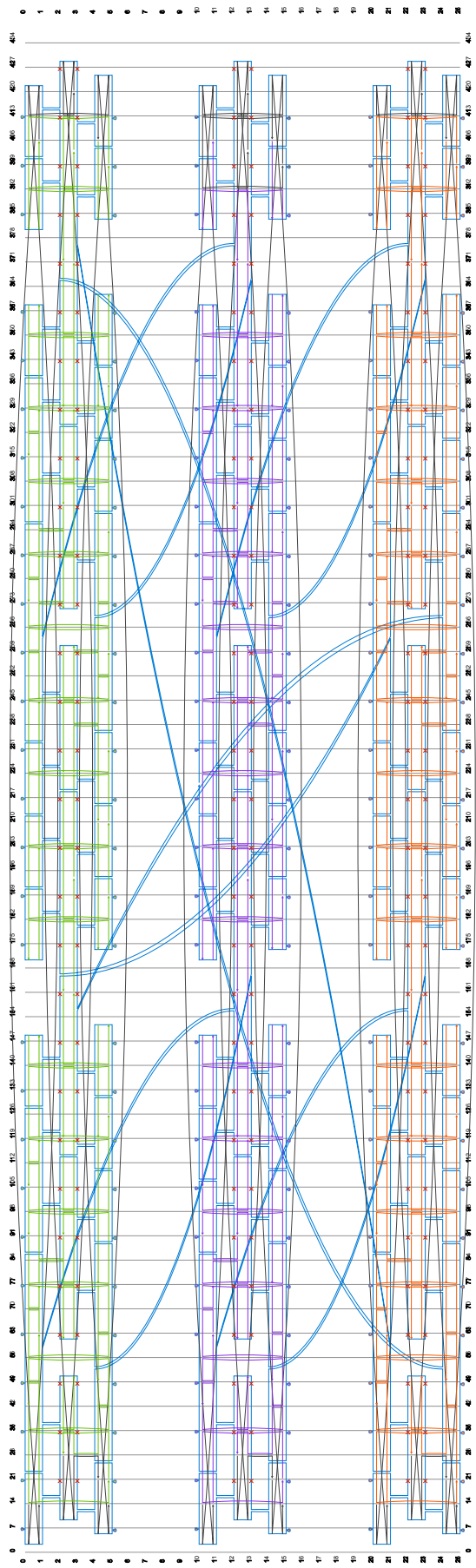
gear 180°



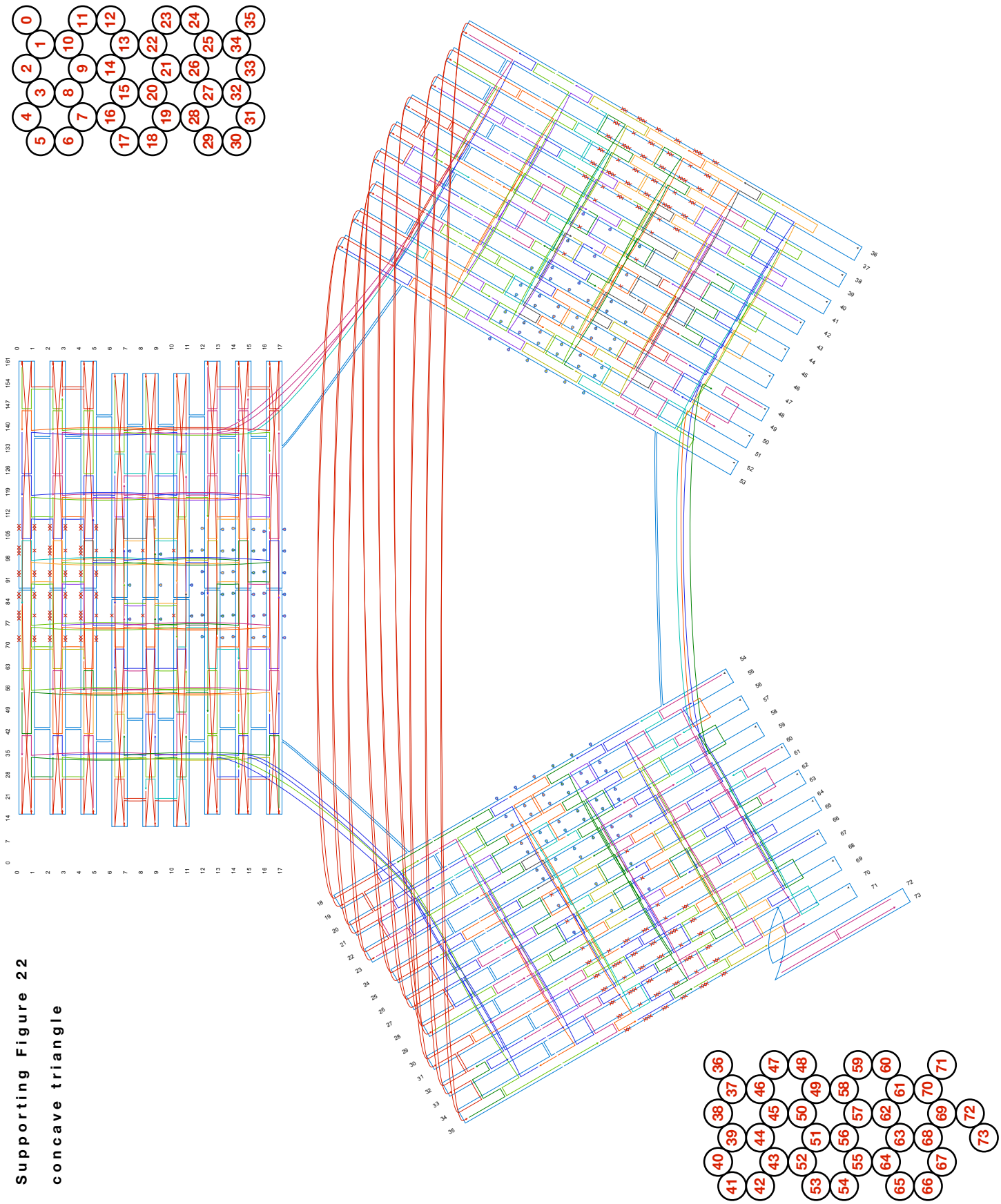
Supporting

Figure 21

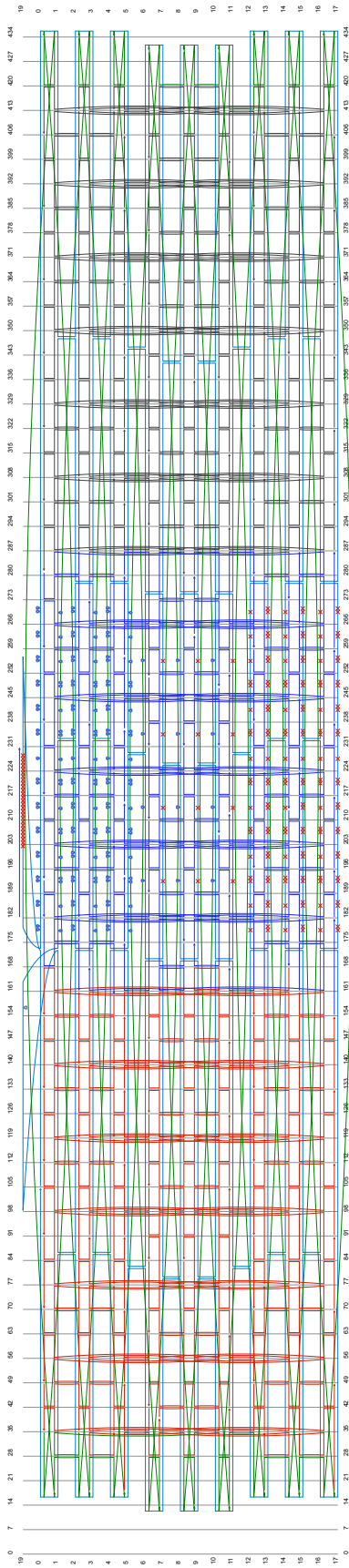
beach ball



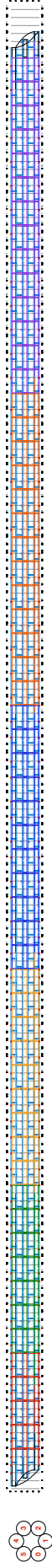
Supporting Figure 22
concave triangle



Supporting Figure 23
convex triangle

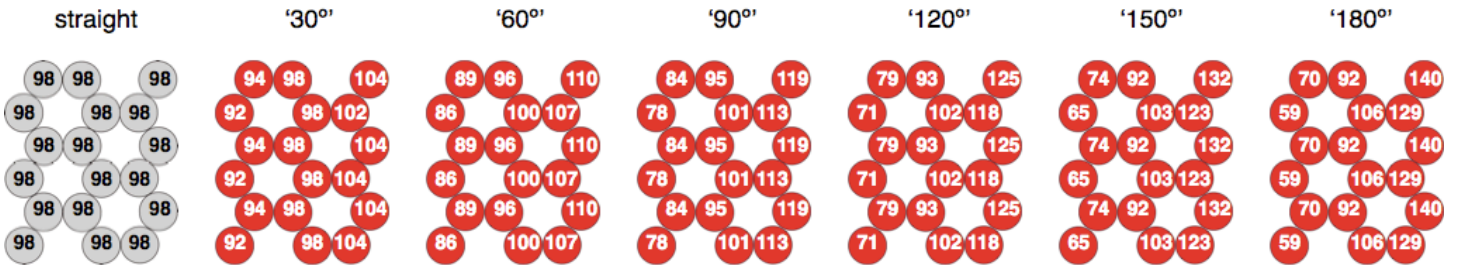


Supporting Figure 24 - Spiral



Supporting Figure 25

Programmed basepair-content between 15 crossover planes (default/straight: 14 x 7 bp = 98 bp)



Programmed # of deletions/insertions distributed between 15 crossover planes (default/straight: 14 x 7 bp = 98 bp)

